Heliyon 10 (2024) e33956

Contents lists available at ScienceDirect

Heliyon

journal homepage: www.cell.com/heliyon

Research article

Removal of tritiated water molecules by isotope exchange reaction between H_2O vapor and tritium water

Takahiro Matsumoto [a,b,*], Chiyori Sakuragawa [a], Tong Mu [a], Koki Tachibana [a], Masashi Ishihara [c], Makoto Tomita [d], Hidehiko Sugimoto [e]

[a] Graduate School of Design and Architecture, Nagoya City University, Nagoya, 464-0083, Japan
[b] Graduate School of Medical Sciences, Nagoya City University, Nagoya, 464-0083, Japan
[c] Laboratory of Radioisotope Research, Nagoya City University, Nagoya, 467-8601, Japan
[d] Department of Physics, Faculty of Science, Shizuoka University, Shizuoka, 422-8529, Japan
[e] Department of Physics, Faculty of Science and Engineering, Chuo University, Tokyo, 112-8551, Japan

ARTICLE INFO

Keywords:
Tritium water
Isotope
Exchange reaction
Purification
Nuclear fusion
Nuclear fission

ABSTRACT

Developing a cost-effective method for separating and concentrating tritium water (HTO) from light water (H_2O) without consuming additional energy is crucial for achieving reliable and safe nuclear fission and fusion energy technologies. However, this presents a significant challenge because of the difficulties in obtaining basic information, such as the chemical and physical properties of HTO molecules. Here, we investigate the isotope exchange reaction (IER) between HTO molecules in H_2O solution and H_2O vapor in the atmosphere. The reduction and purification rates of HTO-containing water were measured by varying the system conditions, such as temperature (20–50 °C) and humidity (50 %–90 %), under an equilibrium state between the liquid phase (water) and vapor phase (air). Our findings indicate that the concentration of HTO in the solution can be significantly reduced by increasing H_2O vapor in the atmosphere. This result can be quantitatively explained by considering the entropy of mixing between the solution and vapor phases. The results obtained here provide both basic understanding on the exchange process between liquid- and vapor-water molecules and a passive technology for treating HTO-containing water.

1. Introduction

Tritium is a radioactive isotope of hydrogen that decays by beta emission. It has a physical half-life of 12.3 years [1,2] and a maximum emission energy of 18.6 keV (average energy of 5.7 keV) [3]. Tritium is naturally produced through nuclear reactions caused by cosmic rays in the atmosphere [4,5]. Annual tritium production is approximately 10^{16}–10^{17} Bq [4,6]. The artificial tritium production exceeds natural production and is caused by nuclear fission reactors, nuclear weapons testing, and decommissioning activities, including dismantling and spent fuel reprocessing [6–9]. Large quantities of tritium have been released into rivers, lakes, oceans, and the atmosphere at levels below national legislation limits [10]. However, this amount is expected to increase with new fission reactors and the realization of future fusion energy [11–14].

Various studies have been conducted on technologies to separate and concentrate tritium from contaminated water and/or air,

* Corresponding author. Graduate School of Design and Architecture, Nagoya City University, Nagoya, 464-0083, Japan.
E-mail address: matsumoto@sda.nagoya-cu.ac.jp (T. Matsumoto).

https://doi.org/10.1016/j.heliyon.2024.e33956
Received 5 April 2024; Received in revised form 30 June 2024; Accepted 1 July 2024
Available online 3 July 2024

including distillation methods [15,16], Girdler sulfide processing [17], electrolysis methods [18,19], catalytic isotope exchange methods [20–22], and functional nanomaterial usage [23,24]. These technologies are important for solving current and future nuclear power problems and reducing the tritium that is continuously discharged into the natural environment. However, these technologies use high concentrations of tritium, large amounts of energy and/or expensive catalysts or materials; therefore, an economical and efficient separation and concentration method (ecosystem) has yet to be developed. This is because hydrogen isotopes have nearly identical molecular sizes, shapes, and thermodynamic properties [25,26]. Therefore, to separate very low concentration of tritiated water (HTO) molecules from environmental water or air systems, a fundamental understanding of HTO molecules such as chemical and physical properties is required. Specifically, the isotope exchange reaction (IER) between HTO and H_2O molecules must be understood to achieve efficient separation.

The IER considered here is a vapor-liquid exchange process involving evaporation and condensation expressed by the following reaction:

$$H_2O\ (\text{liquid}) + \text{HTO}\ (\text{vapor}) \rightleftarrows H_2O\ (\text{vapor}) + \text{HTO}\ (\text{liquid}). \tag{1}$$

This is known as an isotope exchange reaction between HTO vapor and water [27]. The equilibrium constant κ for this reaction is expressed as

$$\kappa = \exp\left(\frac{37813.2}{T^2} - \frac{136.751}{T} + 0.124096\right), \tag{2}$$

and is approximately $\kappa = 1.09$ at $T = 303$ K, as reported by Van Hook [28]. The HTO molecules can be concentrated in H_2O liquid using this low equilibrium constant. However, this low value of κ suggests that the concentration of dilute-HTO vapor into the liquid phase using the reaction from left to right is inefficient, and the concentration requires considerable energy and time.

This study investigates the following IER process from right to left: the exchange reaction between HTO molecules in an H_2O solution and H_2O vapor in the atmosphere. The equilibrium constant in this direction is approximately 1 at room temperature and using H_2O vapor in the atmosphere minimizes the partial pressure of the HTO vapor. Here we investigate the fundamental aspects of this IER process and try to explore the possibility of purifying a large quantity of dilute HTO solution using atmospheric humidity. To attain this possibility, the reduction and purification rates of HTO-containing water were measured by varying the system conditions, such as temperature (20−50 °C) and humidity (50 %–90 %), under an equilibrium state between the liquid phase (water) and vapor phase (air). A quantitative explanation for this result is based on the entropy of mixing between the solution and vapor phases. According to the thermodynamic analysis, the IER process can be controlled by varying the amount of H_2O vapor injected into the system. Consequently, the results obtained here provide a fundamental understanding of the exchange processes between liquid and vapor water molecules using HTO. Furthermore, we consider that the IER process elucidated here leads to a safe and efficient passive technology for treating HTO-containing water discharged from a nuclear power plant and collecting future nuclear fusion resources.

2. Materials and methods

2.1. Model of the exchange reaction between H_2O and HTO molecules at the interface of water

The surface level of the water does not change under saturated vapor pressure because the condensation and evaporation processes between the vapor and liquid phases are in equilibrium. However, the dynamic motion of H_2O molecules at the interface on the order of picoseconds to nanoseconds shows frequent exchange reactions between the liquid and vapor. For instance, at 300 K, approximately 250 mol of water vapor molecules collide with 1 m^2 of water surface per second [29,30]. Although most of these molecules are reflected, some are absorbed by the water surface. This exchange reaction occurs in H_2O molecules and its isotope molecules, such as HTO, as shown in Fig. 1. By successively introducing clear water vapor onto the surface of the HTO-containing water, the number of HTO molecules in the HTO-containing water is reduced; thus, purifying the solution (see Supplemental information V1). The degree of purification of HTO-containing water can be quantitatively explained by considering the entropy of mixing between the liquid and

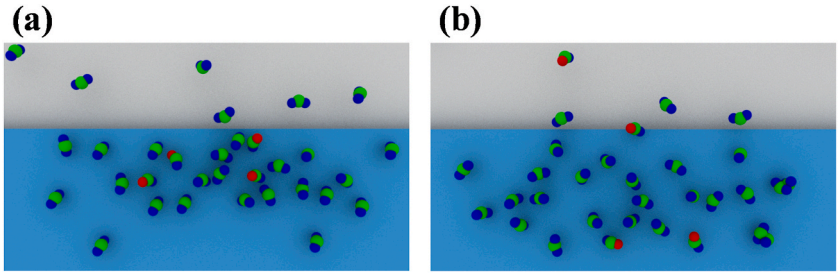

Fig. 1. Model for exchange reaction. (a) H_2O molecules (vapor) entering the water surface. Most of them are reflected, while some are absorbed. (b) Exchange reaction between H_2O and HTO at the water surface. The number of HTO molecules in the HTO-containing water is reduced and purification occurs.

vapor phases, as shown in the following thermodynamic analysis.

2.2. Formulation of HTO and H_2O exchange reactions: Thermal equilibrium state model

We consider the vapor-liquid interface to be in thermal equilibrium. In this case, the number of H_2O and HTO molecules in the vapor-liquid system as a function of duration t can be described as

$$N_1(t) = N_{1v}(t) + N_{1l}(t), \tag{3}$$

$$N_2 = N_{2v}(t) + N_{2l}(t), \tag{4}$$

where subscripts 1, 2, l, and v denote H_2O molecules, HTO molecules, liquid phase, and vapor phase, respectively, $N_1(t)$ and N_2 are the total number of H_2O and HTO molecules, respectively, and N_2 takes a constant value. (We do not consider the physical half-life of 12.3 years during the experiments.) When the system is in equilibrium, the vapor pressure P can be described by the equation of state for an ideal gas as follows:

$$P_1 V = N_{1v} k_B T, \tag{5}$$

$$P_2 V = N_{2v} k_B T, \tag{6}$$

where k_B is Boltzmann constant, V (cm^3) is the volume, and T (K) is the temperature of the system. By applying Raoult's law for H_2O liquid and Henry's law for liquid HTO, the equilibrium vapor pressure can be described as

$$P_1 = P_1^0 \frac{N_{1l}}{N_{1l} + N_{2l}}, \tag{7}$$

$$P_2 = P_2^0 \gamma_{12} \frac{N_{2l}}{N_{1l} + N_{2l}}, \tag{8}$$

where P_1^0 and P_2^0 are the equilibrium vapor pressures of pure H_2O and HTO, respectively, and γ_{12} is a constant calculated from the chemical potentials and interaction energy between the H_2O and HTO molecules in the liquid. Referring to the equilibrium constant in Ref. 28, we assume

$$\frac{\left|P_1^0 - P_2^0 \gamma_{12}\right|}{P_1^0} \ll 1. \tag{9}$$

Using Eq. (9), the following equation can be obtained under the equilibrium conditions:

$$\frac{N_{2l}(t)}{N_{1l}(t)} = \frac{N_{2v}(t)}{N_{1v}(t)} = \frac{N_{2l}(t) + N_{2v}(t)}{N_{1l}(t) + N_{1v}(t)} = \frac{N_2}{N_1(t)}. \tag{10}$$

Therefore, we can purify the HTO-containing water (decrease the rate of N_{2l}/N_{1l}) by increasing the amount of H_2O vapor (increase the molar number of N_{1v}). To quantitatively evaluate N_{1v}, we consider the H_2O-vapor-injection model described in Fig. 2. We increase the volume of the vapor phase (represented by the light-gray-colored cylinder) with a velocity of $v^{(T)}$ while maintaining thermal equilibrium at temperature T (K). The increase in volume results in the introduction of H_2O vapor from the reservoir (that is, H_2O vapor

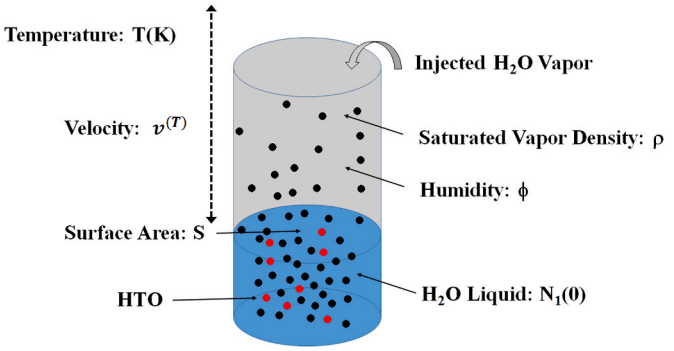

Fig. 2. Theoretical model to calculate isotope exchange reaction (IER) using H_2O vapor injection. Red and black circles represent HTO and H_2O molecules, respectively. Volume of the vapor phase (light-gray-color cylinder) is increased with velocity $v^{(T)}$ while maintaining thermal equilibrium. When the temperature of the system is T (K) and initial H_2O liquid molar number of $N_1(0)$, the amount of H_2O vapor can be calculated as the product of the saturated vapor density ρ (mol/cm^3), relative humidity Φ, surface area S (cm^2), velocity $v^{(T)}$, and duration t (h). (For interpretation of the references to color in this figure legend, the reader is referred to the Web version of this article.)

enters from outside the system). When the temperature of the system is T (K), the amount of H_2O vapor in the volume $N_{1v}(t)$, can be calculated by multiplying the saturated vapor density $\rho^{(T)}$ (mol/cm^3), relative humidity Φ, HTO-containing-water-surface area S (cm^2), velocity $v^{(T)}$ (cm/h), and duration t (h) as follows:

$$N_{1v}(t) = \Phi\, \rho^{(T)}\, S\, v^{(T)}\, t. \tag{11}$$

Substituting Eq. (11) into Eq. (10), the normalized reduction rate of HTO-containing water as a function of the duration $\eta(t)$ can be expressed as

$$\eta(t) = \left(\frac{N_{2l}(t)}{N_{1l}(t)}\right) \Big/ \left(\frac{N_{2l}(0)}{N_{1l}(0)}\right) = \frac{1}{1 + \Phi\rho^{(T)} S\, v^{(T)} t / N_1(0)}, \tag{12}$$

where $N_1(0)$ is the initial number of H_2O molecules in water. Eq. (12) represents that HTO-containing water can be purified by the amount of injected water vapor expressed by Eq. (11). We note here that the same result of Eq. (12) can be obtained based on the reaction rate analysis described in Eq. (1). To determine the IER velocities $v^{(T)}$ as a function of temperature, as in Eq. (11), we performed experiments by varying the system temperature from 20 to 50 °C. After experimentally determining the velocities, we conducted S- and Φ-dependence measurements to confirm the validity of Eq. (12).

2.3. Experimental setup for HTO and H_2O exchange reactions

Fig. 3 shows the experimental setup for the HTO and H_2O IER measurements. Water containing HTO at a concentration of 18.5 GBq/mL (ART0194; American Radiolabeled Chemicals, Inc. St. Louis, Missouri, USA) was diluted with purified water with resistivity above 18 MΩcm (Milli-Q Advantage, Merck KGaA, Darmstadt, Germany) to obtain 250 mL of HTO-containing water at a concentration of 1.67 MBq/L. HTO-containing water was placed in a constant-temperature and constant-humidity chamber (STC-V, SANPLATEC Corp. Osaka, Japan). We varied the temperature and humidity inside the chamber from 20 to 50 °C and 50 %–90 %, respectively. We also varied the surface area of HTO-containing water using beakers of different sizes ranging from 80 to 160 mm in diameter to confirm the assumption described in Eq. (11). To provide clear H_2O vapor to the HTO-containing-water surface, the HTO-containing vapor was removed through an exhaust hood using a dry scroll pump (IDP-3, Varian-Agilent Technologies Corp. California, USA). A flow controller (FS-25 N_2, YAMATO SANGYO Corp. Osaka, Japan) was used to control the evacuation flow rate and maintain thermal equilibrium. The HTO-containing vapor was cooled into water liquid. A Graham condenser (COG-031525, AS ONE Corp. Osaka, Japan) was used to evaluate the amount of water vapor injected into the system. The HTO concentration in the HTO-containing water (high- and low-concentration beakers in Fig. 3) was measured by collecting 100 μL of the solution from the water and then dissolving it in a 5 mL liquid scintillation cocktail (Monofluor LS-191-2, National Diagnostics, Georgia, USA). The mixture was then placed in a low-diffusion polyethylene vial (6000477, PerkinElmer, Connecticut, USA). A liquid scintillation counter (LSC-6000; Nippon RayTech Co., Ltd. Tokyo, Japan) was used for the measurements. The accuracy of the experimental system such as temperature is ±1.0 °C and that of humidity is ±3.0 %. All experiments were performed at least three times independently and all data were expressed as the mean ± standard deviation. All experiments were performed with permission (#23–426) from the Isotope Research Laboratory of Nagoya City University.

3. Results

3.1. Temperature dependence of IER velocity measurements (Φ = 90 % and S = 200 cm^2)

The temperature dependence of IER velocity ($v^{(T)}$) measurements was performed between 20 and 50 °C at a humidity of 90 %, and surface area of 200 cm^2. Fig. 4(a) shows the normalized reduction rate of HTO in HTO-containing water as a function of exchange time

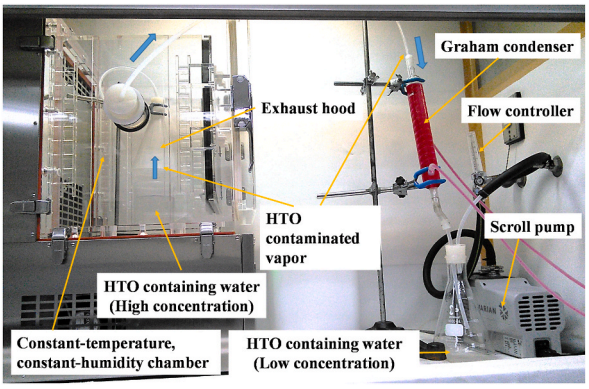

Fig. 3. Experimental setup for HTO and H_2O exchange reaction measurements.

under the above conditions. The blue, green, brown, and red circles represent the experimentally observed reduction rates at 20, 30, 40, and 50 °C, respectively. The reduction rate increases with increasing temperature. The solid lines represent the theoretically fitted curves, as described by Eq. (12), with IER velocity of $v^{(20^{\circ}C)} = 3530$ (cm/h), $v^{(30^{\circ}C)} = 5120$ (cm/h), $v^{(40\ ^{\circ}C)} = 7609$ (cm/h), and $v^{(50\ ^{\circ}C)} = 10718$ (cm/h). The IER reaction velocity becomes larger as the temperature increases. The values of IER velocities and saturated vapor pressures [29,31] are provided in Supplemental information (Table S1). The fitted curves described the experimental results well, indicating the validity of Eq. (12). The magnitude of the exchange reaction obtained using this system is interesting. For example, at 30 °C [$v^{(30\ ^{\circ}C)} = 5120$ (cm/h), $\rho^{(30\ ^{\circ}C)} = 1.69 \times 10^{-6}$ (mol/cm^3), humidity $\Phi = 90$ %, and surface area $S = 200$ cm^2], after 100 h, approximately 155 mol of H_2O vapor will be absorbed into the liquid and the same amount of HTO-containing H_2O water molecules will evaporate from the liquid.

3.2. Surface area dependence measurements ($T = 30$ °C and $\Phi = 90$ %)

Surface area dependence measurements were performed by using polypropylene beakers with diameters of 80 mm (S_1: 50 cm^2), 112 mm (S_2: 100 cm^2), and 160 mm (S_3: 200 cm^2) at 30 °C and a humidity of 90 %. Fig. 4(b) shows the normalized reduction rate as a function of exchange time at the surface area of S_1 (blue circles), S_2 (green circles), and S_3 (red circles). The reduction rate increases with increasing the surface area. The solid lines represent the theoretically fitted curves described in Eq. (12) for the three surface areas. All these curves were fitted by the unique parameter determined by the previous temperature dependence experiments, with $v^{(30\ ^{\circ}C)} = 5120$ (cm/h), $\rho^{(30\ ^{\circ}C)} = 1.69 \times 10^{-6}$ (mol/cm^3), $\Phi = 0.9$, and $N_1(0) = 13.9$ mol. The fitted curves accurately describe the experimental results. The agreement between the experimental results and theoretical curves shows a strong correlation between the reduction rates and surface area.

3.3. Humidity dependence measurements ($T = 30$ °C and $S = 50$ cm^2)

Humidity dependence measurements were performed by changing the humidity level from 50 % to 90 % at 30 °C and a surface area of 50 cm^2. Fig. 4(c) shows the normalized reduction rate as a function of exchange time at relative humidity levels of 50 % (blue circles), 70 % (green circles), and 90 % (red circles). The reduction rate increases with increasing humidity. The solid lines represent the theoretically fitted curves described in Eq. (12) for each humidity level ($\Phi = 0.5$, 0.7, or 0.9) with $v^{(30\ ^{\circ}C)} = 5120$ (cm/h), $\rho^{(30\ ^{\circ}C)} = 1.69 \times 10^{-6}$ (mol/cm^3), $N_1(0) = 13.9$ mol, and surface area $S = 50$ cm^2. The fitted curves accurately describe the experimental results. The agreement between the experimental results and theoretical curves shows a strong correlation between the reduction rates and humidity.

3.4. Supply rate plots

We performed temperature-, surface area-, and humidity-dependence experiments. The experimental results indicate that the reduction rates are accurately described by Eq. (12). Here, to describe these experimental results in a unified manner, we introduce the variable ξ, which represent the supply rate of the water vapor introduced into the liquid system as

$$\xi = \frac{1}{N_1(0)} \Phi \rho^{(T)} S v^{(T)} t. \tag{13}$$

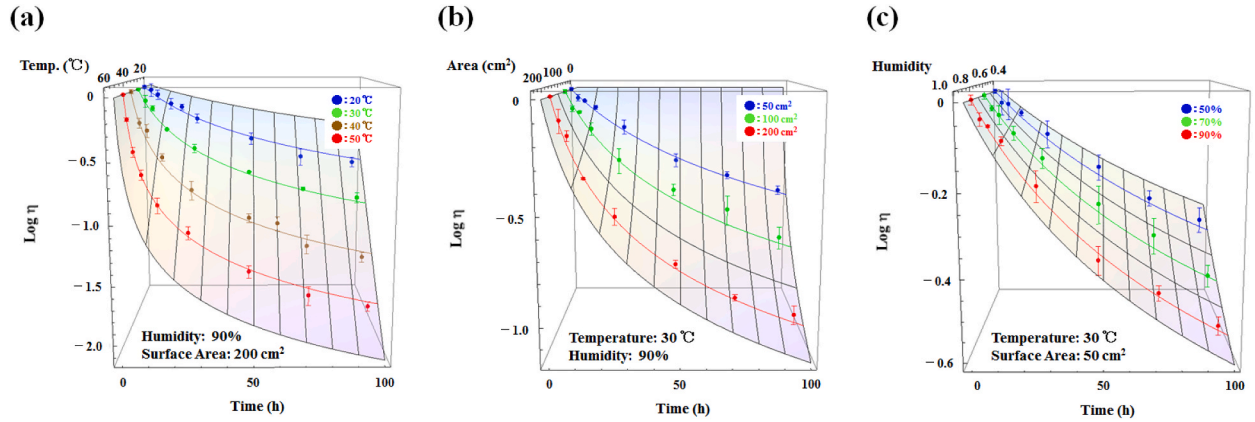

Fig. 4. Time-dependent reduction rates of HTO in HTO-containing water versus (a) temperature: 20 °C (blue circles), 30 °C (green circles), 40 °C (brown circles) and 50 °C (red circles); (b) surface area: 50 cm^2 (blue circles), 100 cm^2 (green circles), and 200 cm^2 (red circles); and (c) humidity: 50 % (blue circles), 70 % (green circles), and 90 % (red circles). (For interpretation of the references to color in this figure legend, the reader is referred to the Web version of this article.)

Using Eq. (13), Eq. (12) can be simplified to $\eta(\xi) = 1/(1+\xi)$, and each reduction rate obtained from the previous experiments (Sections 3.1 to 3.3) can be fitted by a single curve. Fig. 5 shows all the plots of reduction rates η as a function of ξ, where ξ was calculated by putting the experimental conditions of $N_1(0)$, $v^{(T)}$, $\rho^{(T)}$, S, Φ, and t, into Eq. (13). The solid circles, squares, and rhombus represent the points obtained from the temperature-dependence- (Section 3.1), surface-area- (Section 3.2), and humidity-dependence-experiments (Section 3.3), respectively. The plots of reduction rates as a function of ξ align completely with the theoretical curve of $\eta(\xi) = 1/(1+\xi)$ over a wide range of regions from small ($0 \leqq \xi \leqq 20$; as shown in the inset) to large ($0 \leqq \xi \leqq 100$) values. This alignment strongly suggests that the purification of HTO-containing water is governed by the IER between liquid- and vapor-water molecules and that the magnitude of reduction increases at large ξ.

4. Discussion

The exchange reaction described in this paper likely occurs continuously in the HTO storage tanks at the Fukushima nuclear power plant. Here we quantitatively evaluate the IER velocities in the Fukushima HTO storage tank, $v_F^{(T)}$, based on the IER model. We use the following equation, considering a physical half-life of $\tau = 12.3$ years:

$$\eta_F(t) = \frac{(1/2)^{t/\tau}}{1 + \Phi\rho^{(T)} S\, v_F{}^{(T)} t/N_F(0)}, \tag{14}$$

where $\eta_F(t)$ is the normalized reduction rate of the HTO-containing water in the Fukushima HTO storage tank, $N_F(0)$ is the initial number of H_2O molecules in the tank, and t is the time elapsed between HTO concentration measurements. Using Eq. (14) and the reported concentration values of 6.19×10^5 Bq/L in Ref. [32] and 5.38×10^5 Bq/L in Refs. [33,34], we calculate the velocity $v_F^{(13.4°C)}$ as 200 cm/h. This calculation assumed an average temperature of $T = 13.4$ °C [35], $\rho = 6.47 \times 10^{-7}$ mol/cm^3 [31], $\Phi = 69$ % [35], $S = 1 \times 10^6$ cm^2 [36], $N_F(0) = 5.6 \times 10^7$ mol [36], and $t = 17520$ h (2 years from 2021 to 2023) [32–34]. This velocity shows that although the tanks are well sealed, achieving a perfect seal, such as a vacuum vessel, is challenging, and that IERs occur over an extended period at the low reaction velocity. There is a minimal air exchange between the interior and exterior atmospheres of the tank, possibly reducing the concentration of HTO in the storage tank to 1/10 in 34 years as shown by the red curve in Fig. 6. The reduction rates for various IER velocities are also shown in Fig. 6; for example, $v_F^{(13.4°C)}$ as 0 cm/h (perfect seal), the rate is shown by the blue line, 200 cm/h by the red line, 2000 cm/h by the green line, 10000 cm/h by the pink line, and 20000 cm/h by the brown line. The velocity of $v_F^{(13.4°C)} = 200$ cm/h was obtained from the IER experiments conducted here and the average values of temperature and humidity recorded throughout the year. However, it is important to note that temperature and humidity levels can vary significantly depending on the season and location. Therefore, we consider that on-site evaluation is necessary to accurately determine this velocity.

A comparison of the energy savings achievable through the proposed method with those achievable through the conventional evaporation method is required. Based on the values reported in Refs. [37] and [38], it is assumed that each nuclear power plant

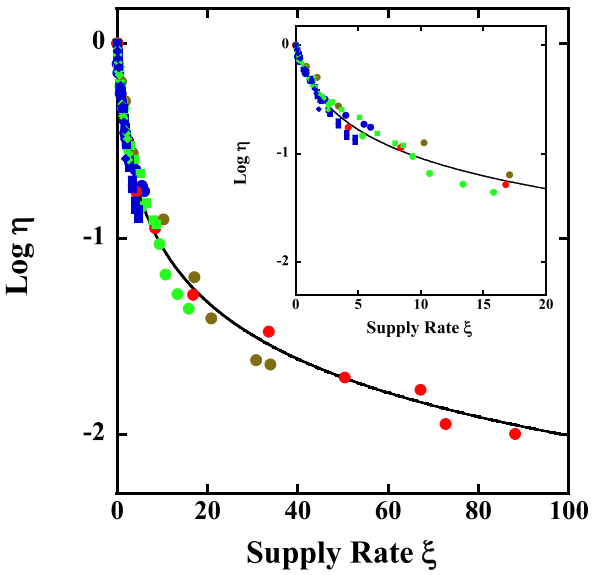

Fig. 5. Reduction rate of HTO plotted against supply rate ξ. Solid circles are points from the temperature dependence experiments, where blue, green, brown, and red circles represent 20, 30, 40, and 50 °C, respectively. Solid squares are points from the surface area dependence experiments, where blue, green, and red squares represent 50, 100, and 200 cm^2, respectively. Solid rhombus are points from the humidity dependence experiments, where blue, green, and red rhombus represent 50 %, 70 %, and 90 %, respectively. (For interpretation of the references to color in this figure legend, the reader is referred to the Web version of this article.)

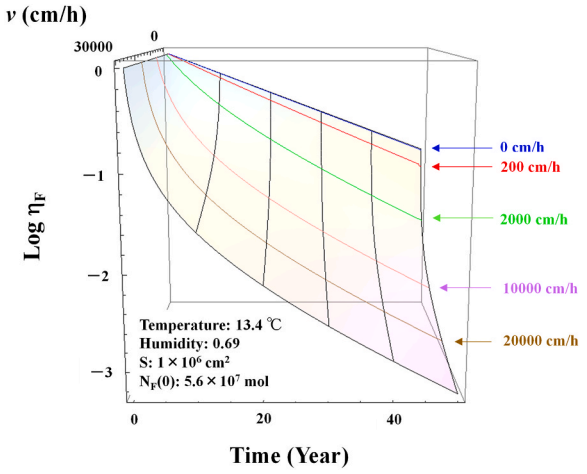

Fig. 6. HTO concentration reduction rates as a function of adjusting the airtightness. $v_F^{(13.4^\circ C)}$ as 0 cm/h (perfect seal), the rate is shown by blue line, 200 cm/h by red line, 2000 cm/h by green line, 10000 cm/h by pink line, and 20000 cm/h by brown line. (For interpretation of the references to color in this figure legend, the reader is referred to the Web version of this article.)

evaporates 10^4 m^3 of tritiated water per year with a concentration of 10^6 Bq/L. In this case, the total amount of energy required to evaporate is approximately 10^{13} J. (It requires 1 J to treat 1 Bq tritium.) When we assume the environmental conditions of $T = 13.4$ °C, $\Phi = 69$ %, and $v_F^{(13.4\ ^\circ C)} = 20000$ cm/h discussed above, and that we can prepare $S = 1 \times 10^8$ cm^2, the concentration of 10^6 Bq/L can be reduced to 6×10^4 Bq/L after one year by the IER. In environments with higher temperature, humidity, and wind speed, the purification velocity increases, allowing for the treatment of a smaller area. To implement the IER method described here, it is necessary to consider various aspects, including meteorological conditions, the required treatment time, and cost-effectiveness.

The enrichment of HTO is an open question. To solve this problem, the diverse functionalities within metal hydrides and nanomaterials make them promising candidates for separating and storing tritium [23,24]. In particular, the surface of hydrogen-terminated nanocrystalline silicon (n-SiH) has been investigated to separate deuterium efficiently [39]. Based on the previous results [39–41], we can expect the efficient exchange reaction occurring between the surface of n-SiH and HTO vapor, such as n-SiH (Solid) + HTO (Vapor) ⇄ n-SiT (Solid) + H_2O (Vapor). The rate of this reaction from left to right was theoretically calculated to be larger than that from right to left by more than one order of magnitude [39–41]. Therefore, this simple exchange process on the n-SiH surface, which is based on the second most abundant element in the Earth, may provide a more sustainable, economical, and environmentally friendly method for tritium enrichment. This protocol, using n-Si, is currently under investigation and will be reported elsewhere.

Interphase mass transfer at the liquid-vapor interface of water is a fundamental process that impacts many areas of physical science, engineering, and biology [42]. However, despite intensive research, the reported evaporation and condensation coefficients [43] differ three order of magnitude [44,45] and there is currently no consensus as to the rate. Based on our results by using HTO molecules, the evaporation coefficient, ε_E [42,43], can be estimated as $\varepsilon_E = 1 \times 10^{-4}$ at 30 °C, which is approximately the same value as that is previously observed [44,45]. To determine the coefficients correctly, we are currently planning a closed system experiment; for example, HTO transfer measurement between a HTO containing water and a purified water in a closed system. Furthermore, we are currently investigating the use of Hofmeister ions [46,47] on the effect of IER. Because the evaporation and condensation process can be controlled by the Hofmeister ions. For example, NaI shows the largest evaporation rate and Na_2HPO_4 shows the smallest evaporation rate [46,47]. Both the determination of the coefficients and the effects of Hofmeister ions on the IER by using HTO molecules are under investigation and will be reported elsewhere.

5. Conclusion

This study determined IER velocities between HTO in H_2O solvent and atmospheric water vapor under various environmental conditions. The results obtained here were quantitatively analyzed by the IER mechanism using thermodynamic calculations. Introducing H_2O vapor onto the surface of HTO-containing water can purify the water without consuming significant energy or time compared to generally used water evaporation discharging. The method presented here offers energy saving approach for treating HTO-containing water discharged from a nuclear power plant and for developing future nuclear fusion technology. The low-temperature treating process compared to the high-temperature vapor discharges may facilitate the handling of tritium-containing water and mitigates corrosion deterioration of nuclear equipment; for example the deterioration of Zr alloys caused by high temperature and humidity conditions [48,49]. Furthermore, we consider that the results obtained in this study may provide fundamental information on the simulation of global circulation of HTO between the ocean and the atmosphere [4,9,50].

Data availability statement

Data will be made available on request.

CRediT authorship contribution statement

Takahiro Matsumoto: Writing – review & editing, Writing – original draft, Project administration, Funding acquisition, Conceptualization. **Chiyori Sakuragawa:** Visualization, Resources, Investigation, Data curation. **Tong Mu:** Software, Resources, Methodology, Data curation. **Koki Tachibana:** Methodology, Investigation, Data curation. **Masashi Ishihara:** Resources, Methodology, Conceptualization. **Makoto Tomita:** Writing – review & editing, Supervision, Formal analysis. **Hidehiko Sugimoto:** Writing – review & editing, Supervision, Formal analysis, Conceptualization.

Declaration of competing interest

The authors declare that they have no known competing financial interests or personal relationships that could have appeared to influence the work reported in this paper.

Acknowledgments

The authors thank Miwako Fujimura (Nagoya City University) for assistance with the liquid scintillation counter measurements. This study was partially supported by the JSPS KAKENHI (grant no. 20H04455).

Appendix B. Supplementary data

Supplementary data to this article can be found online at https://doi.org/10.1016/j.heliyon.2024.e33956.

References

[1] L.L. Lucas, M.P. Unterweger, Comprehensive review and critical evaluation of the half-life of tritium, J. Res. Natl. Inst. Stand. Technol. 105 (2000) 541–549.
[2] A.V. Grosse, W.M. Johnston, R.L. Wolfgang, W.F. Libby, Tritium in nature, Science 113 (1951) 1–2.
[3] C.M. Lederer, V.S. Shirley, Table of Isotopes, seventh ed., Wiley Interscience, New York, 1978.
[4] P.E. Oms, P. Bailly du Bois, F. Dumas, P. Lazure, M. Morillon, C. Voiseux, C. Le Corre, C. Cossonnet, L. Solier, P. Morin, Inventory and distribution of tritium in the oceans in 2016, Sci. Total Environ. 656 (2019) 1289–1303.
[5] B.I. Synzynys, O.A. Momot, O.A. Mirzeabasov, A.V. Zemnova, E.R. Lyapunova, Y.M. Glushkov, A.A. Oudalova, Radiological problems of tritium, KnE Eng. 3 (2018) 249.
[6] M.F. Ferreira, A. Turner, E.L. Vernon, C. Grisolia, L. Lebaron-Jacobs, V. Malard, A.N. Jha, Tritium: its relevance, sources and impacts on non-human biota, Sci. Total Environ. 876 (2023) 162816.
[7] O. Péron, C. Gégout, B. Reeves, G. Rousseau, G. Montavon, C. Landesman, Anthropogenic tritium in the loire river estuary, France, J. Sea Res. 118 (2016) 69–76.
[8] S.B. Kim, M. Bredlaw, H. Rousselle, M. Stuart, Distribution of organically bound tritium (OBT) activity concentrations in aquatic biota from eastern Canada, J. Environ. Radioact. 208–209 (2019) 105997.
[9] B. Nie, S. Fang, M. Jiang, L. Wang, M. Ni, J. Zheng, Z. Yang, F. Li, Anthropogenic tritium: inventory, discharge, environmental behavior and health effects, Renew. Sust. Energ. Rev. 135 (2021) 110188.
[10] Canadian Nuclear Safety Commission, Radioactive release data from Canadian Nuclear Power Plants 2001-10. ISBN: 9781100199092, https://publications.gc.ca/collections/collection_2012/ccsn-cnsc/CC172-13-2010-eng.pdf.
[11] G. Larsen, D. Babineau, D. An evaluation of the global effects of tritium emissions from nuclear fusion power, Fusion Eng. Des. 158 (2020) 111690.
[12] C. Rety, R. Gilbin, E. Gomez, E, Induction of reactive oxygen species and algal growth inhibition by tritiated water with or without copper, Environ. Toxicol. 27 (2010) 155–165, 2012.
[13] S.H. Hong, A review of DEMO reactor concepts: open questions and issues, AAPPS Bull. 32 (2022) 10.
[14] D.J. Hill, Nuclear energy for the future, Nature Mater 7 (2008) 680–682.
[15] S. Fukuda, Tritium isotope separation by water distillation column packed with silica-gel beads, J. Nucl. Sci. Technol. 41 (2004) 619–623.
[16] P. Kowalczyk, P.A. Gauden, A.P. Terzyk, S. Furmaniak, Impact of the carbon pore size and topology on the equilibrium quantum sieving of hydrogen isotopes at zero coverage and finite pressures, J. Phys. Condens. Matter 21 (2009) 144210.
[17] H.K. Rae, Selecting heavy water processes, Am. Chem. Soc. 68 (1978) 1–26.
[18] M. Saito, Enrichment reliability of solid polymer electrolysis for tritium water analysis, J. Radioanal. Nucl. Chem. 275 (2008) 407–410.
[19] S. Ando, T. Komatsuzaki, M. Okada, N. Kataoka, Effects of additives and electrolytic treatment to remove tritium from contaminated water, Heliyon 9 (2023) e17031.
[20] T. Sugiyama, A. Takada, Y. Morita, K. Kotoh, K. Munakata, A. Taguchi, T. Kawano, M. Tanaka, N. Akata, Dual temperature dual pressure water-hydrogen chemical exchange for water detritiation, Fusion Eng. Des. 98–99 (2015) 1876–1879.
[21] G. Ionita, C. Bucur, I. Spiridon, I. Stefanescu, An assessment on hydrogen isotopes separation by liquid phase catalytic exchange process, J. Radioanal. Nucl. Chem. 305 (2015) 117–126.
[22] I.A. Alekseev, S.D. Bondarenko, O.A. Fedorchenko, T.V. Vasyanina, K.A. Konoplev, E.A. Arkhipov, T.V. Voronina, A.I. Grushko, A.S. Tchijov, V.V. Uborsky, Heavy water detritiation by combined electrolysis catalytic exchange at the experimental industrial plant, Fusion Eng. Des. 69 (2003) 33–37.
[23] D. Sun, R. Li, Mi Wen, X. Zhang, M. Chen, H. Yang, D. Guan, C. Xu, G. Zhang, Hydrogen isotopic water separation in membrane distillation through BN, MoS_2 and their heterostructure membranes, Sep. Purif. Technol. 314 (2023) 123634.
[24] M. Rethinasabapathy, S.M. Ghoreishian, S. Hwang, Y. Han, C. Roh, Y.S. Huh, Recent progress in functional nanomaterials towards the storage, separation, and removal of tritium, Adv. Mater. 35 (2023) 2301589.
[25] G. Han, Y. Gong, H. Huang, D. Cao, X. Chen, D. Liu, C. Zhong, Screening of metal–organic frameworks for highly effective hydrogen isotope separation by quantum sieving, ACS Appl. Mater. Interfaces 10 (2018) 32128–32132.

[26] J.Y. Kim, H. Oh, H.R. Moon, Hydrogen isotope separation in confined nanospaces: carbons, zeolites, metal–organic frameworks, and covalent organic frameworks, Adv. Mater. 31 (2019) 1805293.
[27] M. Benedict, T.H. Pigford, H.W. Levi, Nuclear Chemical Engineering, second ed., McGraw-Hill, New York, 1981.
[28] W.A. Van Hook, Vapor pressures of the isotopic waters and ices, J. Phys. Chem. 72 (1968) 1234–1244.
[29] W. Wagner, A. Pruss, The IAPWS formulation 1995 for the thermodynamic properties of ordinary water substance for general and scientific use, J. Phys. Chem. Ref. Data 31 (2002) 387–535.
[30] F. Jones, Evaporation of Water: with Emphasis on Applications and Measurements, CRC Press, New York, 1992.
[31] G.W.C. Kaye, T.H. Laby, Tables of Physical Constants, sixteenth ed., National Physical Laboratory, Hertfordshire, U. K, 1995.
[32] Tokyo Electric Power Company Holdings (TEPCO), Inc., Overview of the basic policy regarding the disposal of water treated by multi-nuclide removal equipment at the Fukushima daiichi nuclear power station of Tokyo electric power company holdings. https://www.tepco.co.jp/decommission/information/committee/roadmap_progress/pdf/2021/d210427_04-j.pdf#page=81, April 27, 2021..
[33] Tokyo Electric Power Company Holdings (TEPCO), Inc., Regarding discharge of water treated by multi-nuclide removal equipment into the ocean, 4th Fukushima Prefecture Nuclear Power Plant Safety Ensuring Technology Study Group, August 23, 2023https://www.pref.fukushima.lg.jp/uploaded/attachment/591602.PDF [in Japanese].
[34] Ministry of Economy, Trade and Industry, *Overview of measures for decommissioning, contaminated water, and treated water,* Decommissioning, contaminated water, and treated water countermeasures team meeting/secretariat meeting, October 26, 2023. https://www.meti.go.jp/earthquake/nuclear/decommissioning/committee/osensuitaisakuteam/2023/10/10/2-1.pdf [in Japanese].
[35] Japan Meteorology Agency Database, Historical Weather Data at Fukushima Prefecture. www.data.jma.go.jp/obd/stats/etrn/view/nml_sfc_ym.php?prec_no=36&block_no=47595 [in Japanese].
[36] Tokyo Electric Power Company Holdings (TEPCO), Inc., Regarding treated water buffer tank replacement. https://www.da.nra.go.jp/file/NR000101014/000226261.pdf, March 29, 2018..
[37] Autorité de sûreté nucléaire, LIVRE BLANC TRITIUM, Groupes de réflexion menés de mai 2008 à avril 2010, sous l'égide de l'ASN et Bilan annuel des rejets de tritium pour les installations nucléaire de base de 2018 à 2022. https://www.asn.fr/sites/tritium/. (Accessed 23 January 2024) [in French].
[38] International Atomic Energy Agency (IAEA), Canadian National Report for the Convention on Nuclear Safety. https://www.iaea.org/sites/default/files/cns_8th_national_report_-_final_canada.pdf.
[39] T. Matsumoto, I. Nomata, T. Ohhara, Y. Kanemitsu, Determination of localized surface phonons in nanocrystalline silicon by inelastic neutron scattering spectroscopy and its application to deuterium isotope enrichment, Phys. Rev. Mater. 5 (2021) 066003.
[40] O.P. Chikalova-Luzina, T. Matsumoto, Ratio of deuterium to hydrogen termination on silicon surface in aqueous electrolyte solutions, Appl. Phys. Lett. 80 (2002) 4507–4509.
[41] I.P. Ipatova, O.P. Chikalova-Luzina, K. Hess, Effect of localized vibrations on the Si surface concentrations of H and D, J. Appl. Phys. 83 (1998) 814–819.
[42] J.D. Smith, C.D. Cappa, W.S. Drisdell, R.C. Cohen, R.J. Saykally, Raman thermometry measurements of free evaporation from liquid water droplets, J. Am. Chem. Soc. 128 (2006) 12892–12898.
[43] M. Knudsen, Die maximale Verdampfungsgeschwindigkeit des Quecksilbers. (The maximum rate of evaporation of mercury, Ann. Phys. 352 (1915) 697–708.
[44] I.W. Eames, N.J. Marr, H. Sabir, The evaporation coefficient of water: a review, Int. J. Heat Mass Tran. 40 (1997) 2963–2973.
[45] R. Marek, J. Straub, Analysis of the evaporation coefficient and the condensation coefficient of water, Int. J. Heat Mass Tran. 44 (2000) 39–53.
[46] B. Rana, D.J. Fairhurst, K.C. Jena, Investigation of water evaporation process at air/water interface using hofmeister ions, J. Am. Chem. Soc. 144 (2022) 17832–17840.
[47] F. Hofmeister, Zur lehre von der wirkung der salze, Naunyn-Schmiedeberg's Arch. Pharmacol. 25 (1888) 1–30.
[48] International Atomic Energy Agency (IAEA), Corrosion of zirconium alloys in nuclear power plants, IAEA-TECDOC-684 (1993). ISSN 1011-4289.
[49] A.T. Motta, A. Couet, R.J. Comstock, Corrosion of zirconium alloys used for nuclear fuel cladding, Annu. Rev. Mater. Res. 45 (2015) 311–343.
[50] K. Liger, C. Grisolia, I. Cristescu, C. Moreno, V. Malard, D. Coombs, S. Markelj, Overview of the TRANSAT (TRANSversal actions for tritium) project, Fusion Eng. Des. 136 (2018) 168–172.